BNL-224127-2023-JAAM

Polyvinyl Alcohol Anion Exchange Resin Composite Membrane with Co@Cu Core-Shell Particles for Direct Borohydride Fuel Cell Applications

Y. He, M. Ge

To be published in "ACS Applied Energy Materials"

February 2023

Photon Sciences

Brookhaven National Laboratory

U.S. Department of Energy

USDOE Office of Science (SC), Basic Energy Sciences (BES) (SC-22)

DISCLAIMER

A polyvinyl alcohol anion exchange resin composite membrane with Co@Cu core-shell particles for direct borohydride fuel cell applications

Yan He†, Wen Chu‡, Haiying Qin$*, Jiabin Liu‡, Mingyuan Ge#, Xiaojing Huang#, Hanfei Yan#, Yong S. Chu#, Zhaohui Dong†, Aiguo Li†*

†Shanghai Synchrotron Radiation Facility, Shanghai Advanced Research Institute, Chinese Academy of Sciences, Shanghai, 201800, P. R. China

‡ School of Materials Science and Engineering, Zhejiang University, Hangzhou 310027, P. R. China

$ College of Materials and Environmental Engineering, Hangzhou Dianzi University, Hangzhou 310018, P. R. China

National Synchrotron Light Source II, Brookhaven National Laboratory, Upton, New York 11973, USA

KEYWORDS: Direct borohydride fuel cells; Anion exchange membrane; Core-shell structure; Composite membrane; Nanoscale fluorescence X-ray imaging

ABSTRACT: A polyvinyl alcohol anion exchange resin composite membrane, functionalized with Co and Cu ions, is reported for use in direct borohydride fuel cells. The CoCu-functionalized membrane has a 30.5 % lower fuel permeability than that of a blank membrane. Meanwhile, the

cell performance of the direct borohydride fuel cell can also be improved by employing the CoCu-functionalized membrane, reaching a maximum power density of 304 $mW \cdot cm^{-2}$ at 60 °C. High-resolution fluorescence images directly demonstrate the formation of Cu/Co core-shell structure micro-particles in the CoCu membrane, which not only reduces the Co content but increases the active surface area of Co species in CoCu-functionalized membrane, resulting in the improvement of cell performance.

1. INTRODUCTION

In recent decades, fuel cells have attracted extensive attention due to their high performance and low pollution in the electrochemical energy conversion process [1-4]. Among the several types of fuel cells, direct borohydride fuel cells (DBFCs) have gained increasing development because of their potential advantages, such as high electromotive potential, high efficiency of energy conversion, and the possibility of using non-noble metal catalysts [5-8]. However, the poor performance and the conduction-permeability dilemma within anion exchange membranes (AEMs) hinder the commercialization of DBFCs [9].

It is well known that the alkaline system is more suitable for DBFCs than the acidic systems [10, 11]. AEM is a key component of DBFC and plays an important role in DBFC performance. Many researchers are engaged in developing new cost-effective AEMs with high conductivity and low fuel-permeability. A great number of AEMs for DBFCs based on poly (4, 4'-diphenylether-1, 3, 4-oxadiazole) [12], cross-linked chitosan [13, 14], and polyvinyl alcohol [15-17] have been widely explored. Among them, polyvinyl alcohol (PVA) is a cost-effective non-toxic polymer with excellent membrane properties and an ideal matrix for AEMs. A PVA/hydroxyapatite composite membrane was synthesized and applied into a DBFC by Yang et al. [15], which achieved a maximum power

density of 45 mW cm^{-2}. Huang et al. [16] investigated the alkali-doped PVA/carbon nanotubes (PVA/CNTs) electrolyte, which could be a cost-effective alternative for the commercial Nafion membrane in the DBFC. An anion exchange resin (AER)/PVA blend alkaline membrane was developed and applied into alkaline fuel cells such as direct urea fuel cell and direct ammonia fuel cell by Tao et al.[18, 19]. Moreover, some researchers tried to combine the excellent functionality of organics and the stability of inorganics by preparing various organic-inorganic composite AEMs. A poly (arylene ether sulfone)/nano-ZrO_2 composite membrane with outstanding properties was fabricated by Li et al. [20]. In addition, the power density of fuel cells could also be enhanced by using metal ions-introduced PVA membranes. For example, the power density of fuel cells effectively increases from 39 mW cm^{-2} to 87.8 mW cm^{-2} after the doping of Fe_3O_4 into the PVA membrane [21, 22].

In our previous work, a CoOOH-functionalized PVA membrane has been successfully synthesized, which has shown an excellent performance (144 mW cm^{-2} at 30 °C) for application in DBFC [23]. To further decrease the Co loading and increase the hydroxide conductivity, core-shell Cu@Co additives are in-situ synthesized within the membrane in this work. During the preparation, half of the expensive $CoSO_4$ was replaced by the relatively cheap $CuCl_2$. Such core-shell structure of Cu@Co is found to play an crucial role in improving the performance of DBFCs.

2. EXPERIMENTAL

The $CoSO_4$-functionalized membrane was synthesized by mixing three commercial compounds (a commercial strong anion exchange resin (AER) (Amberlite IRA-402(OH)), hydroxide form, Alfa Aesar), $CoSO_4 \cdot 7H_2O$ (Alfa Aesar), and PVA (MW 57000-66000, Alfa Aesar) at a weight ratio of 125:4:250. Firstly, PVA was added to the $CoSO_4$ solution. The mixture was then stirred at

95 °C for 2 hours to form a gel, after which the gel-solution mixture was cooled to 40 °C. Then the commercial AER was grounded into powder and added into the mixture to form the wet composite polymer gel. The synthesized polymer gel was then spread on a glass plate and dried naturally to form the $CoSO_4$-functionalized membrane (hereafter labeled as Co-AEM). The core-shell Cu@Co functionalized membrane (hereafter labeled as CoCu-AEM) was fabricated similarly but changing the weight ratio to 125:2:2:250 by replacing half portion of $CoSO_4$ with $CuCl_2$. For comparison, a blank membrane without $CoSO_4$ and $CuCl_2$ was similarly prepared and studied as well (blank AEM). The dried membranes were finally immersed into a 1 M KOH solution for 24 h before being used as the electrolyte membranes in DBFCs.

The fuel (borohydride ion) permeability of the membrane was tested in a side-by-side diffusion cell at 25 °C [9]. Both sides were first filled with 50 mL 0.1 M NaOH solution, and then 0.1 M $NaBH_4$ was added to the middle permeating chamber. The extent of borohydride ions transport through the membrane was determined by the concentration of borohydride in sampling solutions from the receiving compartment in certain time intervals, using the spectrophotometric method proposed by Werner et al. [24]. The permeability (P) was calculated via the equation based on the slope of the BH_4^- concentration against elapsed time [16]:

$$P = (\text{slope})\frac{LV}{CA} \qquad (1)$$

where L is the thickness of the membrane, V is the volume of the receiving compartment, C is the initial borohydride concentration in the source compartment, and A is the effective permeation area of the membrane.

The single-cell performance was performed at a fuel flow rate of 10 $mL \cdot min^{-1}$ and a humidified O_2 flow rate of 50 mL·min-1 under 0.2 MPa using a PFX-2011 battery tester (Kikusui Electronics Corp.). The tests were carried out at temperatures of 30 and 60 °C. An alkaline $NaBH_4$ solution

containing 5 wt.% of $NaBH_4$ and 10 wt.% of NaOH was used as the fuel. The cell configuration had an active area of 6 cm^2, and the testing details could be found in reference [25]. Polypyrrole-modified carbon-supported cobalt hydroxide ($Co(OH)_2$-PPy-BP) was used as the catalyst for both anode and cathode with a loading of 5 and 3 $mg \cdot cm^{-2}$, respectively. The preparation details of $Co(OH)_2$-PPy-BP could be found in reference [25].

The crystal structures of Co- and CoCu-AEMs were characterized by synchrotron radiation X-ray diffraction (XRD) with incident X-ray energy of 20 keV, which was performed at BL15U1 of Shanghai Synchrotron Radiation Facility (SSRF). High-resolution mapping of Co and Cu distribution in CoCu-AEM and Co-AEM samples using nanoscale X-ray fluorescence imaging was conducted at Hard X-ray Nanoprobe Beamline (HXN) [26, 27] at National Synchrotron Light Source-II (NSLS-II) of the Brookhaven National Laboratory. The monochromatic X-rays at 10.4 keV were focused to a spot size of ~50 nm × ~50 nm by using a Fresnel X-ray Zone plate. The X-ray fluorescence imaging measurements (XRF) were conducted by collecting the emitted fluorescence X-rays using a three-element silicon drift detector (Vortex 3ME) while scanning the sample with a continuous fly-scan mode. Element distribution images were obtained by fitting the scanning fluorescence spectra using the X-ray fluorescence analysis software PyXRF [28].

Ptychography imaging was conducted simultaneously with the X-ray fluorescence imaging [29], by collecting the far-field diffraction patterns. The data were analysed using an iterative phase-retrieval algorithm to produce the morphological image of the sample. Fig. 1 shows the schematic diagram of the experimental layout of combined fluorescent and ptychographic imaging.

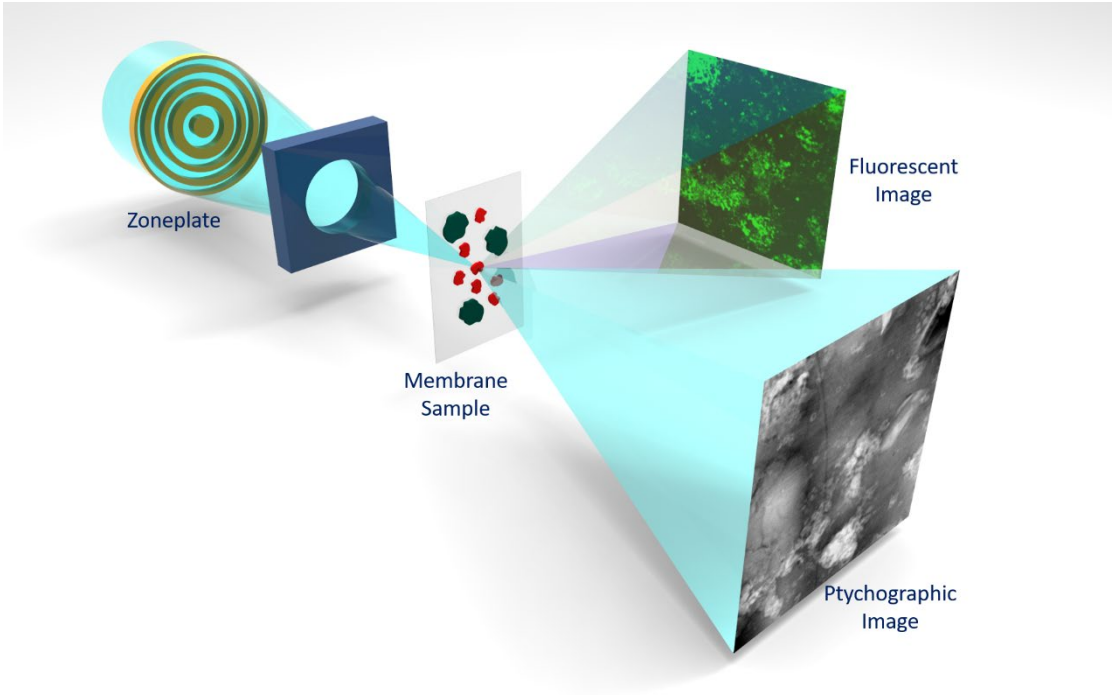

Figure 1. A schematic diagram of the experimental layout of combined fluorescent and ptychographic imaging.

The obtained complex-valued image represents the sample transmittance functions with an achievable spatial resolution better than the focal size. The pixelated area detector with 55 μm pitches was placed at 0.5 m downstream of the specimen. A 96 × 96 pixel was cropped and fed into 100 iterations of ptychography reconstruction with the difference map algorithm [30]. The pixel size of the reconstructed image is ~12.7 nm. The periodic artifact was partially removed by filtering the periodic satellite peaks in Fourier space [31].

3. RESULTS

The XRD patterns of Co-AEM and CoCu-AEMs are illustrated in Fig. 2(a). The diffraction reflections at approximately 11.4°, 19.4°, and 40.4° belong to the pure PVA crystalline phase [32, 33]. Similar to the reported Co-doped AEM [21], no crystalline phases relating to Co and Cu

compounds are formed in the membranes. To investigate the effect of Co and Cu additions on the permeability of AEMs, a comparative study was also carried out on blank AEMs fabricated with the same method. Based on the permeability test results in Fig. 2(b), the BH_4^- permeability of Co-AEM and CoCu-AEMs obtained are 2.7×10^{-6} and 2.5×10^{-6} $cm^2 \cdot s^{-1}$, respectively. Comparing with the blank AEM (3.6×10^{-6} $cm^2 \cdot s^{-1}$), the permeability of the membranes doping with Co and CoCu decreased by 25% and 30.5%, respectively. It has been reported that the doping of Co ions into AEM could result in a reduction in BH_4^- permeability via reducing the diffusion coefficient of the membrane [23]. Therefore, the decreasing BH_4^- permeability observed in this study could also be attributed to the additions of metal ions in the membrane. It is known that the doped Co ions can catalyze the hydrolysis of borohydride ions effectively. Some borohydride ions could hydrolyze when permeating the membrane, which decreases the BH_4^- ions across rate in the Co and CoCu-AEMs, leading to the reduction of BH_4^- permeability. Due to the lower costs, less fuel diffusing, and lower unwelcome mixed over-potential on the cathode, the performance of DBFC would benefit from the use of CoCu-AEM.

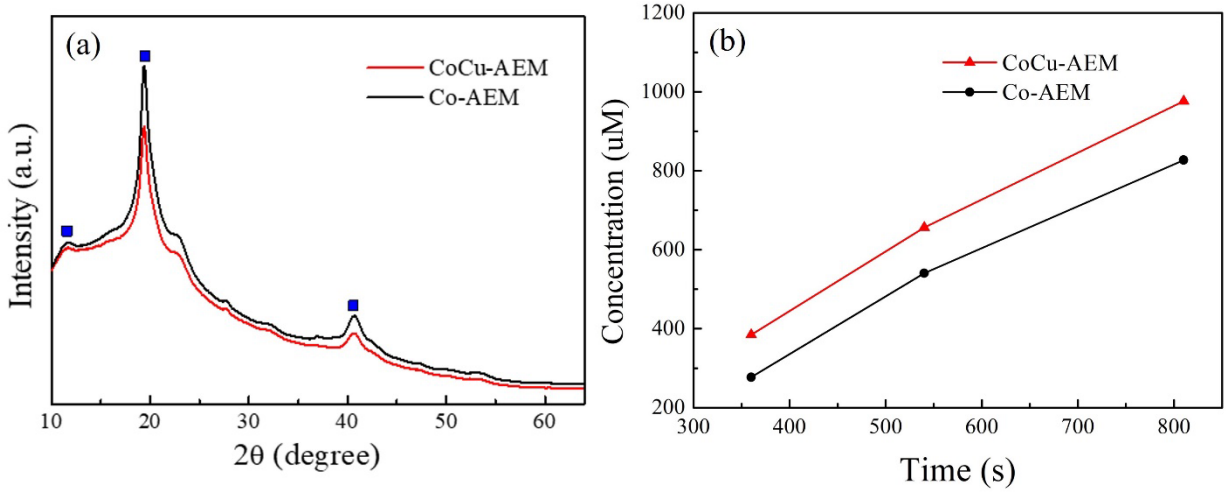

Figure 2. (a) XRD spectrum of the Co-AEM and CoCu-AEM, (b) the change of BH_4^- concentration with time, from which the permeabilities of Co-AEM and CoCu-AEM are calculated.

The cell voltages and power densities, measured at 30 and 60 °C, as a function of the current densities of the DBFCs with Co- and CoCu-AEMs are illustrated in Fig. 3(a-d). The operating voltages for both DBFCs decrease gradually with the increasing current densities, and the open-circuit voltages of both two DBFCs are close to 1.1 V. The P_{max} of the CoCu-AEM assembled DBFC reaches 190 mW·cm^{-2} at 30 ºC and 304 mW·cm^{-2} at 60 ºC, which are much higher than that of DBFC with Co-AEM (165 and 283 mW·cm^{-2}). To best of our knowledge, the highest reported P_{max} of DBFCs using NaOH-doped PVA membranes was 96 mW·cm^{-2} [16]. As shown in Fig. 3(c), the P_{max} of DBFC using CoCu-AEM is higher than that using Co-AEM, unaffected by the operation temperatures (30 and 60 °C). It indicates that the doping of inactive Cu species to a certain extent can effectively and surprisingly enhance the DBFC performance. More efforts are needed to figure out the enhancing mechanisms of the doped Cu ions in CuCo-AEM.

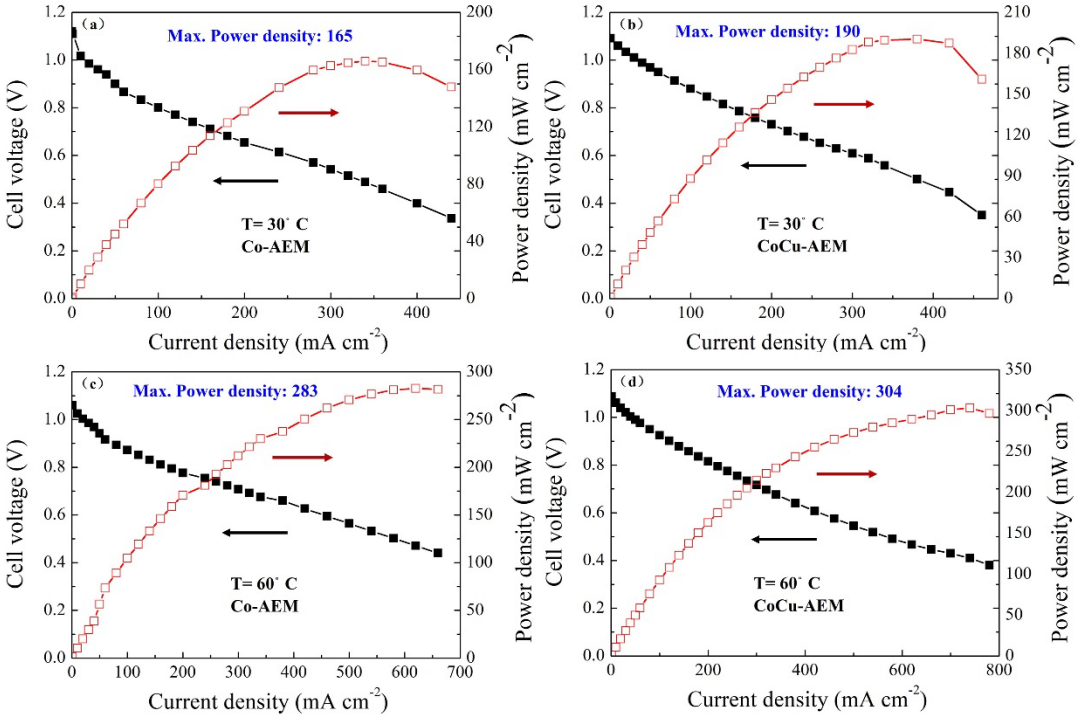

Figure 3. The cell performance of DBFCs using Co-AEM (a) (c) and CoCu-AEM (b) (d) as electrolytes at 30 and 60 ºC, respectively.

Generally, the ORR catalytic activity of the Cu element is lower than the Co element, which means the Cu-AEM usually has a higher permeability than that of Co-AEM. Thus, it is interesting to find the co-doping of Co, and Cu ions further decrease the BH_4^- permeability of AEM by 5.5% comparing with Co-AEM. Meanwhile, the cell performance of the DBFC using co-doping AEM was also significantly increased, even though half of Co ions were replaced by the inactive Cu species.

To elucidate the enhancing mechanisms of DBFC using co-doping AEM, X-ray fluorescence and ptychographic imaging were conducted simultaneously on Co-AEM and CoCu-AEMs. These two methods are complementary to each other. Elemental and morphological distributions are imaged, by each method. The fluorescence mapping of Co ions shows that the Co ions unevenly dispersed in the Co-AEM and formed the Co-enriched clusters (as indicated in Fig. 4(a)). Such Co-rich clusters are most likely caused by the strong magnetism of Co ions to the quaternary ammonium groups on the resins in the matrix. With the high resolution of the fluorescence mapping, obvious size differences can be seen in the Co-enriched clusters. The ptychographic reconstruction of the Co-AEM membrane shows the phase image (proportional to the electronic density) of the membrane as illustrated in Fig. 4(b). Fig. 4(c) shows the merged image of the fluorescence image of Co distribution and the ptychographic image of the membrane, which yields a clear visual representation of the Co ions distribution within the membrane. The merged image suggests that the Co-enriched clusters are preferred to gather on the surface of the membrane rather than distribute inside the membrane. However, the fluorescence mapping image merged with the

ptychographic image of CoCu-AEM shows a smooth surface with Co ions evenly distributed inside the membrane (as shown in Fig. 5). In strong contrast to Co-ions, fluorescence mapping results of Cu ions in CoCu-AEM show dispersed Cu particles with the size of 1-3 µm. The merged overlay image of Co and Cu elemental distributions clearly illustrates the core-shell structure of CoCu particles in the CoCu-AEM.

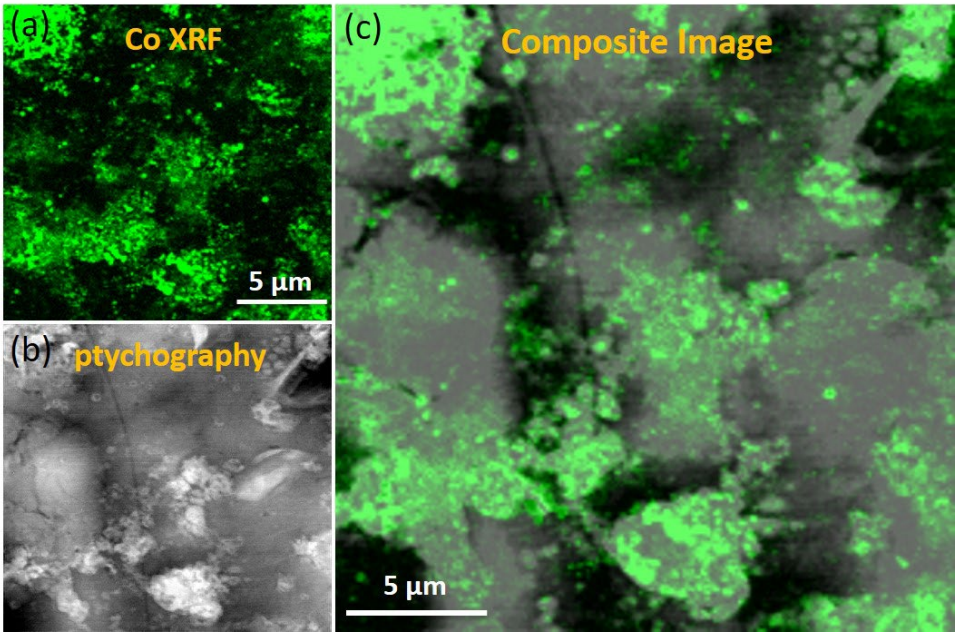

Figure 4. Images of the Co-AEM from scan data collected at HXN beamline. (a) The X-ray fluorescence map of the distribution of the element Co in the membrane. (b) The phase image of membrane reconstructed via ptychography. (c) The fluorescence image of Co distribution merged on the ptychographic image.

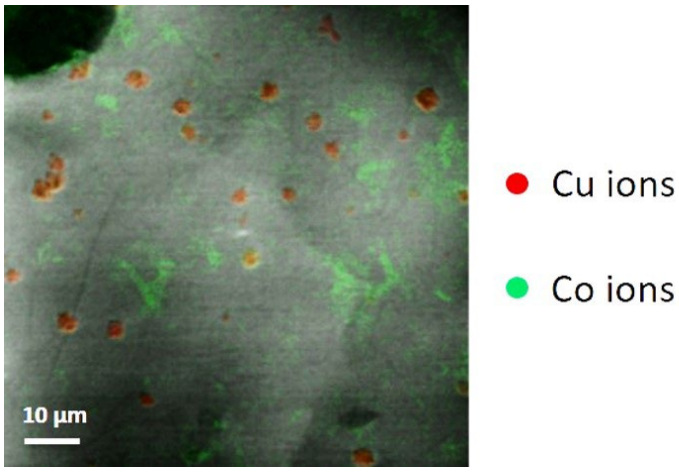

Figure 5. The merged overlay fluorescence images of Co and Cu elemental distributions and ptychographic image.

To confirm the structure of CoCu core-shell particles, fluorescence mapping of a single CoCu particle with a higher spatial resolution of 30 nm was performed. The high-resolution images of a single CoCu particle randomly selected from the Fig.5 are shown in Fig. 6(a) and 6(b). The distributions of Co and Cu elements around a CoCu-particle show that both ions have similar shapes. However, when images of Co and Cu-ions are merged, the Cu fluorescence signals were found localized in the center, while Co signals appeared near the outer region of the particle. In addition, a line profile of the Co and Cu concentration (in Fig. 6(d)) was extracted at the position marked by a dashed line in Fig. 6(c) to compare their concentration profiles The Cu-ion density displays a Gaussian-like profile, which is a reasonable approximation of a projected density of a sphere. This suggests that Cu ions are evenly distributed throughout the particle. Strongly different from Cu-profile, the Co-ions have a relatively flat-top profile, which means the distribution of Co-ion is independent of the depth or bulky of the particle. In other words, the Co ions are only accumulated on the surface of the Cu-Co particle. Together with the merged XRF images, these observations demonstrated that the CoCu particle has a core-shell structure of Cu core and Co

shell. Moreover, according to the profiles of Co and Cu domains, the core-shell particle shows an approximate 100 nm Co shell around a 2 μm Cu core. To further confirm it, different areas of the membrane were searched, and similar distribution of Co and Cu within the area with several micrometers was observed. Thus, it can be confirmed that the CoCu micro-particle is composed of a Cu core and a Co shell, regardless of the particle size.

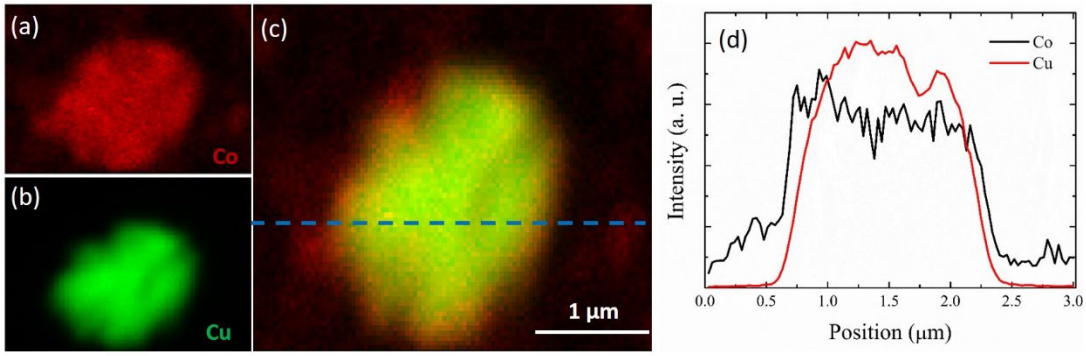

Figure 6. High-resolution XRF images of (a) Co and (b) Cu domains in a single particle randomly selected from the Fig.5. (c) The merged overlay XRF image of Co and Cu to show the core-shell structure. (d) The intensity profile was obtained at a position marked by a dashed line in (d).

This phenomenon is mainly related to the different binding modes of different cations with resin and PVA. According to previous studies, Cu ions tend to adsorb on the surface of alkaline resin powders, while the transition metal ions (such as Co ions) are easier to complex with PVA. It can be inferred that Cu ions are more easily hydrolysed and form a nuclear structure with the quaternary ammonium groups of the resin than Co ions. The complex formed by Co^{2+} and PVA is more stable and becomes a relatively dispersed shell structure. Due to the different properties of cations, the simple preparation process of such binary core-shell structure can be easily extended to prepare various high-performance AEMs. In our previous work [22], it has been demonstrated that the doping

of catalytic Co ions into the membrane can reduce the crossover of borohydride, and thus improve the performance of DBFCs. However, in this study, although half of the active Co species were replaced by inactive Cu ions in CoCu-AEM, the DBFC using CoCu-AEM still possessed higher performance. It is highly possible the cell performance could be improved by increasing the active surface area of Co species in CoCu-AEM and the more hydroxide ions attracted by the Cu core around the resin. Thus, it can be confirmed that arranging Co ions to form thin shells on Cu cores would not only greatly reduce the Co loading, but also significantly enhance the performance of DBFCs.

4. CONCLUSION

In this work, a CoCu-AEM with Cu-Co core-shell structural additives was prepared for the different hydrolysis degrees of cations and was used as an effective electrolyte for DBFCs. Comparing with the Co-AEM, the BH_4^- permeability decreased while the cell performance employing CoCu-AEM was improved. The CoCu particles in the CoCu-AEM have a core-shell structure of Cu core and Co shell according to the high-resolution fluorescence results, owing to the different bonding energies of Co and Cu cations with PVA and resins. The increase of the active surface area of Co species and the accelerated OH^- conduction is concluded as the mechanism for the enhanced properties of CoCu-AEM.

ASSOCIATED CONTENT

AUTHOR INFORMATION

Corresponding Author

*Yan He Shanghai Synchrotron Radiation Facility, Shanghai Advanced Research Institute, Chinese Academy of Sciences, Shanghai, 201800, P. R. China. E-mail: heyan@zjlab.org.cn.

*Haiying Qin College of Materials and Environmental Engineering, Hangzhou Dianzi University, Hangzhou 310018, P. R. China. E-mail: hyqin@hdu.edu.cn.

Give contact information for the author(s) to whom correspondence should be addressed.

Author Contributions

The manuscript was written through contributions of all authors. All authors have given approval to the final version of the manuscript.

Funding Sources

This work is financially supported by the National Key Research and Development Program of China (Grant 2021YFA1601001), the Photon Science Center for Carbon Neutrality of Chinese Academy of Science, and the Zhejiang Provincial Natural Science Foundation of China (No. LZ22B060001).

Notes

Any additional relevant notes should be placed here.

ACKNOWLEDGMENT

This research used the Hard X-ray Nanoprobe Beamline at 3-ID of the National Synchrotron Light Source II, a U.S. Department of Energy (DOE) Office of Science User Facility operated for the DOE Office of Science by Brookhaven National Laboratory under Contract No. DE-SC0012704. This research also used BL15U1 in Shanghai Synchrotron Radiation Facilities (SSRF). This work is financially supported by the National Key Research and Development Program of China (Grant

2021YFA1601001), the Photon Science Center for Carbon Neutrality of Chinese Academy of Science, and the Zhejiang Provincial Natural Science Foundation of China (No. LZ22B060001).

REFERENCES

(1) Steele, B. C. H. and Heinzel, A., Materials for fuel-cell technologies. *Nature* **2001**, *414*, 345-352.

(2) Bashyam, R. and Zelenay, P. A. A Class of non-precious metal composite catalysts for fuel cells, *Nature* **2006**, *443*, 63-66.

(3) Jacobson, M. Z.; Colella, W. G. and Golden, D. M. Cleaning the air and improving health with hydrogen fuel-cell vehicles, *Science* **2005**, *308*, 1901.

(4) Ma, J.; Choudhury, N. A. and Sahai Y., A comprehensive review of direct borohydride fuel cells, *Renew. Sustain. Energy Rev.* **2010**, *14*, 183-199.

(5) Amendola, S. C.; Onnerud, P.; Kelly, M. T.; Petillo, P. J.; Sharp-Goldman, S. L. and Binder, M. A novel high power density borohydride-air cell, *J. Power Sources* **1999***, 84,* 130-133.

(6) Choudhury, N. A.; Ma, J. and Sahai, Y., High performance and eco-friendly chitosan hydrogel membrane electrolytes for direct borohydride fuel cells, *J. Power Sources* **2012**, *210*, 358-365.

(7) Merino-Jiménez, I.; Ponce de León, C.; Shah, A. A. and Walsh, F. C. Developments in direct borohydride fuel cells and remaining challenges, *J. Power Sources* **2012**, *219*, 339-357.

(8) Oshchepkov, A.; Bonnefont, A.; Maranzana, G.; Savinova, E. R. and Chatenet, M. Direct borohydride fuel cells: A selected review of their reaction mechanisms, electrocatalysts, and influence of operating parameters on their performance, *Curr. Opin. Electroche.* **2022**, 32, 100883.

(9) Chu, W.; Jiang, W.; Sheng, H. H.; Yuan, G. Z.; Lin, W. H.; Lin, L. X.; Qin, H. Y.; Meng, L. and Liu, J. B. Fuel permeability of anion exchange membranes under electric field, *Electrochim. Acta*, **2018**, *266*, 357-363.

(10) Liu B.; and Li, Z. Current status and progress of direct borohydride fuel cell technology development, *J. Power Sources* **2009**, *187*, 291-297.

(11) Coowar, F. A.; Vitins, G.; Mepsted, G. O.; Waring, S. C. and Horsfall, J. A. Electrochemical oxidation of borohydride at nano-gold-based Electrodes: Application in direct borohydride fuel cells，*J. Power Sources* **2008**, *175*, 317-324.

(12) Ma, Z.; Zhang, H.; Li, X.; Geng, X.; and Zhang, H. Polymer Electrolyte Based on Chemically Stable and Highly Conductive Alkali-doped polyoxadiazole for direct borohydride fuel cell. *Electrochemistry Communications* **2011**, *13*, 1009-1012.

(13) Ma, J.; Choudhury, N. A.; Sahai, Y. and Buchheit, R. G. A high performance direct fuel cell employing cross-linked chitosan membrane, *J. Power Sources* **2011**, *196*, 8267-8264.

(14) Choudhury, N. A.; Sahai, Y. and Buchheit, R. G. Chitosan chemical hydrogel electrode binder for direct borohydride fuel cells, *Electrochemistry Communications* **2011**, *13*, 1-4.

(15) Yang, C. C.; Li, Y. J.; Chiu, S. J.; Lee, K. T.; Chien, W. C. and Huang, C. A. A direct borohydride fuel cell based on poly(vinyl alcohol)/hydroxyapatite composite polymer electrolyte membrane, *J. Power. Sources* **2008**, *184*, 95-98.

(16) Huang, C. C.; Liu, Y. L.; Pan, W. H.; Chang, C. M.; Shih, C. M.; Chu, H. Y.; Chien, C. H.; Juan, C. H. and Lue, S. J. Direct borohydride fuel cell performance using hydroxide-conducting polymeric nanocomposite electrolytes, *J. Polym. Sci. B Polym. Phys.* **2013**, *51*, 1779-1789.

(17) Wang, Y. J.; Qiao, J.; Baker, R. and Zhang, J. Zhang, Alkaline polymer electrolyte membranes for fuel cell applications, *Chem. Soc. Rev.* **2013**, *42*, 5768-5787.

(18) Lan,R.; Tao, S. W. and Irvine, J. T. S. A direct urea fuel cell - power from fertiliser and waste, *Energy Environ. Sci.* **2010**, *3*, 438-441.

(19) Lan, R. S. and Tao, W. Direct ammonia alkaline anion-exchange membrane fuel cells, *Electrochemical and Solid-State Letters* **2010**,*13*, B83-B86.

(20) Li, X. H.; Yu, Y. F. and Meng, Y. Z. Novel quaternized poly (arylene ether sulfone)/Nano-ZrO_2 Composite anion exchange membranes for alkaline fuel cells, *ACS Appl. Mater. Interfaces* **2013**, *5*, 1414-1422.

(21) Pan, W. H.; Lue, S. J.; Chang, C. M. and Liu, Y. L. Alkali doped polyvinyl alcohol/multi-walled carbon nano-tube electrolyte for direct methanol alkaline fuel cell, *J. Membr. Sci.* **2011**, *376*, 225-232.

(22) Lo, C. F.; Wu, J. F.; Li, H. Y.; Hung, W. S.; Shih, C. M.; Hu, C. C.; Liu, Y. L. and Lue, S. J. Novel poly (vinylalcohol) nanocomposites containing carbon nano-tubes with Fe_3O_4 pendants for alkaline fuel cell applications, *J. Membr. Sci.* **2013**, *444*, 41-49.

(23) Qin, H. Y.; Hu, Y. P.; Zhu, C.; Chu, W.; Sheng, H. H.; Dong, Z. X.; He, Y.; Wang, J.; Li, A. G.; Chi, H. Z.; Ni, H. L.; Ji Z. G. and Liu, J. B. Functionalization of polyvinyl alcohol composite

membrane by CoOOH for direct borohydride fuel cells, *Electrochemistry Communications* **2017**, *77*, 1-4.

(24) Werner, D. A.; Huang, C. C. and Aminoff, D. Micro method for determination of borohydride with nad+, *Anal. Biochem.* **1973**, *54*, 554-560.

(25) Qin, H. Y.; Liu, Z. X.; Ye, L. Q.; Zhu, J.; K.; Li, Z.; P. The use of polypyrrole modified carbon supported cobalt hydroxide as cathode and anode catalysts for the direct borohydride fuel cell, *J. Power Sources* **2009**, *192*, 385-390.

(26) Yan, H.; Bouet, Zhou; N. J.; Huang, X.; Nazaretski, E.; Xu, W.; Cocco, A.; Chiu, W. and Brinkman, K. Multimodal hard x-ray imaging with resolution approaching 10 nm for studies in material science. *Nano Futures* **2018**, *2*, 11001.

(27) Nazaretski, E.; Yan, H.; Lauer, K.; Bouet, N.; Huang, X.; Xu, W.; Zhou, J.; Shu, D.; Hwu, Y.; Chu, Y. S. Design and Performance of an X-ray Scanning Microscope at the Hard X-ray Nanoprobe Beamline of the NSLS-II. 0*J. Synchrotron Rad.* **2017**, *24*, 1113.

(28) Li, L.; Yan, H.; Xu, W.; Yu, D.; Heroux, A.; Lee, W. K.; Campbell, S. I.; Chu, Y. S. PyXRF: Python-based X-ray Fluorescence Analysis Package. *X-Ray Nanoimaging: Instruments and Methods III* **2017**, *10389*, 103890U,.

(29) Lin, R.; Bak, S. M.; Shin, Y.; Zhang, R.; Wang, C.; Kisslinger, K.; Ge, M.; Huang, X.; Shadike, Z.; Pattammattel, A.; Yan, H.; Chu, Y. S.; Wu, J.; Yang, W.; Whittingham, M. S.; Xin, H. L. and Yang, X. Hierarchical Nickel Valence Gradient Stabilizes High-nickel Content Layered Cathode Materials. *Nature Comm.* **2021**, *12*, 2350.

(30) Thibault, P.; Dierolf, M.; Menzel, A.; Bunk, O.; David, C. and Preiffer, F. High-Resolution Scanning X-ray Diffraction Microscopy. *Science* **2008**, *321*, 379-382.

(31) Huang, X.; Yan, H.; Ge, M.; Öztürk, H.; Nazaretsk, E.; Robinson, IK. and Chu, Y. S. Artifact Mitigation of Ptychography Integrated with On-the-fly Scanning Probe Microscopy. *Applied Physics Letters* **2017**, *111*, 023103.

(32) Hong, P. D.; Chen, J. H. and Wu, H. L. Solvent Effect on Structural Change of Poly(vinyl alcohol) Physical Gels. *J. Appl. Polym. Sci.* **1998**, *69*, 2477-2486.

(33) Ma, X. D.; Qian, X. F.; Yin, J. and Zhu, Z. K. Preparation and Characterization of Polyvinyl Alcohol-selenide Nanocomposites at Room Temperature. *J. Mater. Chem.* **2002**, *12*, 663-666.

Table of contents

High-resolution fluorescence images directly demonstrate the formation of Cu/Co core-shell structure micro-particles in the CoCu membrane, which not only reduces the Co content but increases the active surface area of Co species in CoCu-functionalized membrane, resulting in the improvement of cell performance.